Scaling laws of the out-of-time-order correlators at the transition to the spontaneous $\mathcal{PT}$-symmetry breaking in a Floquet system

Wen-Lei Zhao [1,*] Ru-Ru Wang,[1] Han Ke,[1] and Jie Liu [2,3,†]

[1]*School of Science, Jiangxi University of Science and Technology, Ganzhou 341000, China*
[2]*Graduate School, China Academy of Engineering Physics, Beijing 100193, China*
[3]*HEDPS, Center for Applied Physics and Technology, and College of Engineering, Peking University, Beijing 100871, China*

We investigate both numerically and analytically the dynamics of out-of-time-order correlators (OTOCs) in a non-Hermitian kicked rotor model, addressing the scaling laws of the time dependence of OTOCs at the transition to the spontaneous $\mathcal{PT}$-symmetry breaking. In the unbroken phase of $\mathcal{PT}$ symmetry, the OTOCs increase monotonically and eventually saturate with time, demonstrating the freezing of information scrambling. Just beyond the phase transition points, the OTOCs increase in the power laws of time, with the exponent being larger than 2. Interestingly, the quadratic growth of OTOCs with time emerges when the system is far beyond the phase transition points. The above numerical findings are validated by our theoretical analysis, which provides a general framework with important implications for Floquet engineering and information scrambling in chaotic systems.

I. INTRODUCTION

Non-Hermiticity has been regarded as a fundamental modification to the conventional quantum mechanics [1–10], a subclass of which with $\mathcal{PT}$ symmetry even displays the transition from the real energy spectrum to a complex one. Such intrinsic spontaneous $\mathcal{PT}$-symmetry breaking occurs at the exceptional points (EP), at which both the eigenstates and eigenvalues coalesce [11–19]. The existence of EP leads to rich physics, such as the enhancement of precision in quantum sensors [20], the topological phase transition [21–25], the nonadiabatic transition [26,27], and the unidirectional propagation of light [28], just to name a few. Theoretical advances enabled exponential realizations of $\mathcal{PT}$-symmetric systems in various fields, such as optical settings [29–42], electronic circuits [43], and optomechanical systems [44]. Moreover, the extension of Floquet-driven systems to the $\mathcal{PT}$-symmetric regime has opened up unique opportunities for understanding fundamental concepts such as quantum chaos [45] and quantum-classical transition [46,47]. Interestingly, chaos is found to facilitate the scaling law of the spontaneous $\mathcal{PT}$-symmetry breaking in a $\mathcal{PT}$-symmetric kicked rotor (PTKR) model [48]. This system even displays ballistic energy diffusion [49] and the quantized acceleration of momentum current [50], which enriches our understanding on the unique transport phenomena in the presence of chaos.

The dynamics of out-of-time-order correlators OTOCs, originally introduced by Lakin *et al.*, in the study of quasiclassical theory of superconductivity [51], received extensive studies in the fields of high-energy physics [52–54],

condensed matter physics [55–60], and quantum information [61–63]. It was found that OTOCs can effectively detect quantum chaos [64–67], quantum thermalization [68], and information scrambling [69–74]. A paradigmatic model in the field of chaos is the kicked rotor. Investigations on this model have shed light on fundamental problems related to quantum computation [75], quantum control of chaos [76], and many-body chaos [77,78]. The periodic delta-kicking has promising applications in engineering the low-energy dispersion [79] and dynamical localization (DL) [80]. In the semiclassical limit, the exponential growth of OTOCs is governed by the Lyapunov exponent of classical chaos, which demonstrates a route of quantum-classical correspondence [81]. In Floquet-driven systems, OTOCs have been used to diagnose dynamical quantum phase transition [82] and entanglement [83,84]. Intrinsically, we previously found a quantized response of OTOCs when varying the kicking potential of the PTKR model [85]. In a non-Hermitian Ising chain, the Yang-Lee edge singularity dominates the dynamics of OTOCs encircling EP [86]. State-of-the-art experimental advances observed different kinds of OTOCs in the setting of nuclear magnetic resonance [87,88], trapping ions [89], and qubit under Floquet engineering [90].

In this context, we both numerically and analytically investigate the dynamics of OTOCs when the PTKR model is in different phases of $\mathcal{PT}$ symmetry. We use a machine learning method, namely, a long short-term memory network (LSTM), to classify the phase diagram of $\mathcal{PT}$-symmetry breaking and extract the phase boundary in a wide range of system parameters. We find that, in the unbroken phase of $\mathcal{PT}$ symmetry, OTOCs increase monotonically with time evolution and eventually saturate, demonstrating the freezing of operator growth. We analytically prove that the saturation of OTOCs is a power-law function of the real part of the

---
*wlzhao@jxust.edu.cn
†jliu@gscaep.ac.cn

kicking potential. In the broken phase of the $\mathcal{PT}$ symmetry, we find a power-law increase of OTOCs with time, for which the characteristic exponent is larger than 2 when the system is just beyond the phase transition point, and is equal to 2 for the system far beyond the phase transition point. Through the detailed analysis of the wavepacket's dynamics in the time reversal process, we uncover the mechanisms of both the dynamical localization and the power-law increase of OTOCs. Our investigations reveal that the dynamics of OTOCs can be utilized to diagnose spontaneous $\mathcal{PT}$-symmetry breaking.

The paper is organized as follows. In Sec. II, we describe the PTKR model and show the scaling law of spontaneous $\mathcal{PT}$-symmetry breaking. In Sec. III, we show the scaling laws of the dynamics of OTOCs at the transition to the $\mathcal{PT}$-symmetry breaking. Section IV contains the theoretical analysis of the scaling laws of OTOCs. The conclusion and discussion are presented in Sec. V.

II. TRANSITION TO SPONTANEOUS $\mathcal{PT}$-SYMMETRY BREAKING IN FLOQUET SYSTEMS

A. Model

The Hamiltonian of the PTKR model in dimensionless units reads

$$H = \frac{p^2}{2} + V(\theta) \sum_n \delta(t - t_n), \quad (1)$$

where the kicking potential $V(\theta) = K[\cos(\theta) + i\lambda \sin(\theta)]$ satisfies the $\mathcal{PT}$-symmetric condition $V(\theta) = V^*(-\theta)$ [48–50]. The parameters K and λ indicate the strength of the real and imaginary parts of the kick potential, respectively. The $p = -i\hbar_{\text{eff}}\partial/\partial\theta$ is the angular momentum operator, θ is the angle coordinate, and $\hbar_{\text{eff}}$ denotes the effective Planck constant. The time $t_n(= 0, 1, 2 \ldots,)$ is the integer, indicating kicking numbers. The eigenequation of the angular momentum operator is $p|\varphi_n\rangle = n\hbar_{\text{eff}}|\varphi_n\rangle$ with eigenstate $\langle\theta|\varphi_n\rangle = e^{in\theta}/\sqrt{2\pi}$ and eigenvalue $p_n = n\hbar_{\text{eff}}$. On the basis of $|\varphi_n\rangle$, an arbitrary quantum state can be expanded as $|\psi\rangle = \sum_n \psi_n|\varphi_n\rangle$.

For time-periodic systems, i.e., $H(t + T) = H(t)$, the Floquet theory predicts the eigenequation of the evolution operator $U|\psi_\varepsilon\rangle = e^{-i\varepsilon}|\psi_\varepsilon\rangle$, where the eigenphase ε is referred to as quasienergy. One-period time evolution of a quantum state of the PTKR system is given by $|\psi(t_{j+1})\rangle = U|\psi(t_j)\rangle$ with the Floquet operator

$$U = U_f U_K = \exp\left(-\frac{i}{\hbar_{\text{eff}}}\frac{p^2}{2}\right)\exp\left[-\frac{i}{\hbar_{\text{eff}}}V(\theta)\right]. \quad (2)$$

This demonstrates that, in numerical simulations, one period evolution is split into two steps, namely, the kicking evolution U_K and the free evolution U_f. The kick evolution is realized in angle coordinate space, i.e., $\psi'(\theta) = U_K(\theta)\psi(\theta, t_j)$. Then, one can utilize the fast Fourier transform to change the state $\psi'(\theta)$ to angular momentum space, thereby obtaining its component ψ'_n on the eigenstate $|\varphi_n\rangle$. Finally, the free evolution is conducted in angular momentum space, i.e., $\psi_n(t_{j+1}) = U_f(p_n)\psi'_n$. By repeating the same procedure, one can obtain the quantum state at arbitrary time [91].
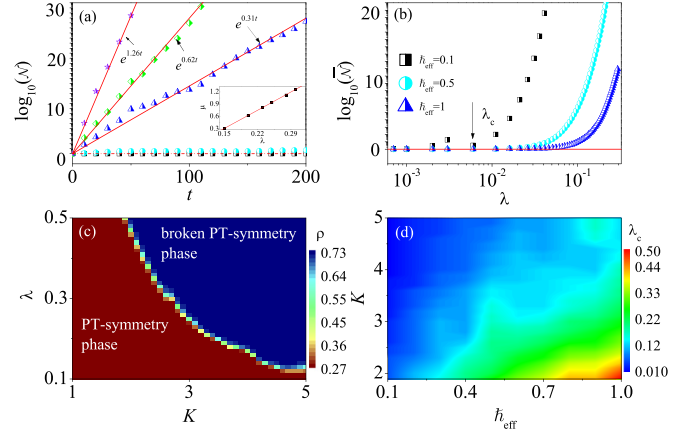

FIG. 1. (a) Norm $\mathcal{N}$ versus time for $\lambda = 0.01$ (squares), 0.05 (circles), 0.15 (triangles), 0.2 (diamonds), and 0.3 (pentagrams). The parameters are $K = 5$ and $\hbar_{\text{eff}} = 1$. Solid lines indicate the exponential increase, i.e., $\mathcal{N}(t) = e^{\mu t}$, while dash-dotted line denotes $\mathcal{N} = 1$. Inset: The μ versus λ. Solid line indicates the linear increase $\mu \propto \lambda$. (b) Average value $\bar{\mathcal{N}}$ versus λ for $K = 5$ with $\hbar_{\text{eff}} = 0.1$ (squares), 0.5 (circles), and 1 (triangles). Solid line denotes $\mathcal{N} = 1$. (c) Phase diagram of the spontaneous $\mathcal{PT}$-symmetry breaking for $\hbar_{\text{eff}} = 1$. One can see clearly a phase boundary λ_c. Here, the value of ρ, generated by a well-trained LSTM network, determines the probability of a parameter value (λ, K) being within the $\mathcal{PT}$-symmetry phase ($\rho = 0$) or the unbroken $\mathcal{PT}$-symmetry phase ($\rho = 1$). (d) The value of λ_c in the parameter space $(K, \hbar_{\text{eff}})$.

B. Spontaneous $\mathcal{PT}$-symmetry breaking

It is straightforward to prove that the Floquet operator of the PTKR satisfies the $\mathcal{PT}$ symmetry $U = (\mathcal{PT})^\dagger U \mathcal{PT}$, where $\mathcal{P}$ and $\mathcal{T}$ are the parity and time reversal operators, respectively. Based on conventional understanding of quantum mechanics, one asserts that the two operators, i.e., U and $\mathcal{PT}$ have simultaneous eigenstates, that is to say, the quasieigenstate $|\psi_\varepsilon\rangle$ is also the eigenstate of the $\mathcal{PT}$ operator, i.e., $\mathcal{PT}|\psi_\varepsilon\rangle = \pm|\psi_\varepsilon\rangle$. This conclusion is indeed valid for positive quasienergies $\varepsilon > 0$. However, a notable feature of the PTKR system is that complex quasienergies $\varepsilon = \varepsilon_r \pm \varepsilon_i$ emerge when the strength of the imaginary part of the complex potential exceeds a threshold value, i.e., $\lambda > \lambda_c$ [48–50]. The threshold value λ_c is just the EP of the system. It can be proven that the quasieigenstate $|\psi_\varepsilon\rangle$ is no longer an eigenstate of the $\mathcal{PT}$ operator due to the complex quasienergies, thus demonstrating the spontaneous $\mathcal{PT}$-symmetry breaking. An intrinsic quality of the PTKR system is that $\mathcal{PT}$ symmetry is helpful in protecting the real spectrum of the Floquet operator.

We assume that the initial state is expanded as $|\psi(t_0)\rangle = \sum_\varepsilon \rho_\varepsilon|\psi_\varepsilon\rangle$. Then, after the nth kick, the quantum state has the expression $|\psi(t_n)\rangle = U^{t_n}|\psi(t_0)\rangle = \sum_\varepsilon \rho_\varepsilon e^{-i\varepsilon_r t_n}e^{\varepsilon_i t_n}|\psi_\varepsilon\rangle$, whose norm $\mathcal{N} = \langle\psi(t_n)|\psi(t_n)\rangle$ exponentially increases with time due to positive ε_i. We numerically investigate the time evolution of $\mathcal{N}$ for different λ. Without loss of generality, we choose a Gaussian wavepacket, i.e., $\psi(\theta, t_0) = (\sigma/\pi)^{1/4}\exp(-\sigma\theta^2/2)$ with $\sigma = 10$ as the initial state in numerical simulations. Figure 1(a) shows that, for very small λ (e.g., $\lambda = 0.01$ and 0.05), the value of $\mathcal{N}$ equals almost to

unity with time evolution, which implies that quasienergies are all real. Interestingly, for sufficiently large λ (e.g., $\lambda = 0.15$), $\mathcal{N}$ increases exponentially with time, i.e., $\mathcal{N} = e^{\mu t}$, and the growth rate μ increases with the increase of λ. The nonunitary feature of the Floquet operator, specifically, the real component of the kicking evolution operator, denoted as $U_K^R = \exp[K\lambda \sin(\theta)/\hbar_{\text{eff}}]$, leads to the growth of the norm. A rough estimation of the norm yields a time dependence of the form $\mathcal{N} \propto \exp(K\lambda t/\hbar_{\text{eff}})$, indicating the relation of the growth rate $\mu \propto \lambda$, which is confirmed by our numerical results [see inset in Fig. 1(a)]. We further investigate the long-time average value of the norm $\bar{\mathcal{N}} = \sum_{n=1}^{N} \mathcal{N}(t_n)/N$ for a wide range of λ. Figure 1(b) shows that, for a specific $\hbar_{\text{eff}}$ (e.g., $\hbar_{\text{eff}} = 0.1$), $\bar{\mathcal{N}}$ remains at unity for λ smaller than a threshold value λ_c, beyond which it monotonically increases with λ. It is reasonable to believe that the threshold value λ_c corresponds to the emergence of spontaneous $\mathcal{PT}$-symmetry breaking.

Recently, the LSTM network was exploited to extract the character of time series and thus to predict the phase diagram of quantum diffusion [92]. Based on the character of the time evolution of $\mathcal{N}$, we conducted supervised training on the LSTM network and used it to evaluate the feature of $\mathcal{N}(t)$, namely, whether $\mathcal{N}(t) = e^{\mu t}$ or not, for different system parameters [93]. This highly effective machine learning method outputs the probability ρ of the time series $\mathcal{N}(t)$ to be exponentially increasing or not, which can predict the phase diagram of spontaneous $\mathcal{PT}$-symmetry breaking. Interestingly, our results show that the ρ increases with the increase of both K and λ [see Fig. 1(c)]. We identify two phases in the parameter's space (K, λ), the boundary of which is clearly visible in Fig. 1(c). We further investigate the λ_c for different K and $\hbar_{\text{eff}}$. Our results demonstrate that the critical parameter λ_c increases with the increase of $\hbar_{\text{eff}}$ and decreases with the increase of K [see Fig. 1(d)]. This behavior is rooted in the fact that the mean spacing level Δ of the quasienergies of the quantum kicked rotor (QKR) model is proportional to $\hbar/K$ [48]. The smaller the Δ is, the easier it is for the non-Hermitian parameter λ to cause the coalescence of two quasienergies, implying the relation $\lambda_c \propto \hbar/K$.

III. SCALING LAWS OF THE OTOCS AT THE TRANSITION TO THE SPONTANEOUS $\mathcal{PT}$-SYMMETRY BREAKING

The OTOCs are defined by $C(t_n) = -\langle[\hat{A}(t_n), \hat{B}]^2\rangle$, with the operators $\hat{A}(t_n) = U^\dagger(t_n)AU(t_n)$ and B being evaluated in the Heisenberg picture [56,61,65,81,94–98]. The average, i.e., $\langle \cdots \rangle = \langle \psi(t_0)| \cdots |\psi(t_0)\rangle$, is taken over an initial state $|\psi(t_0)\rangle$ [99]. In this work, we consider the case where both $\hat{A}$ and $\hat{B}$ are angular momentum operators, i.e., $C(t) = -\langle[p(t), p]^2\rangle$. We use a Gaussian wavepacket, i.e., $\psi(\theta, t_0) = (\sigma/\pi)^{1/4} \exp(-\sigma\theta^2/2)$ with $\sigma = 10$ as the initial state. It is worth noting that, as opposed to static-lattice systems, periodically driven systems have no thermal states, as the temperature grows to infinity with time evolution [100]. Thus, there is no need to average over the initially thermal states in the definition of $C(t_n)$ in our system [85,101].

Straightforward derivation yields the equivalence

$$C(t_n) = C_1(t_n) + C_2(t_n) - 2\text{Re}[C_3(t_n)], \tag{3}$$

where the two-points correlators, namely, the first two terms in right side are defined by

$$C_1(t_n) = \langle\psi_R(t_0)|p^2|\psi_R(t_0)\rangle, \tag{4}$$

$$C_2(t_n) = \langle\varphi_R(t_0)|\varphi_R(t_0)\rangle, \tag{5}$$

and the four-points correlator is

$$C_3(t_n) = \langle\psi_R(t_0)|p|\varphi_R(t_0)\rangle, \tag{6}$$

with $|\psi_R(t_0)\rangle = U^\dagger(t_0, t_n)pU(t_0, t_n)|\psi(t_0)\rangle$ and $|\varphi_R(t_0)\rangle = U^\dagger(t_0, t_n)pU(t_0, t_n)p|\psi(t_0)\rangle$ [102]. The symbol $\text{Re}[\cdots]$ denotes the real part of a complex variable.

To obtain the state $|\psi_R(t_0)\rangle$, three steps must be carried out: (i) the forward evolution from t_0 to t_n, i.e., $|\psi(t_n)\rangle = U(t_0, t_n)|\psi(t_0)\rangle$; (ii) the action of the operator p on the state $|\psi(t_n)\rangle$, i.e., $|\tilde{\psi}(t_n)\rangle = p|\psi(t_n)\rangle$; and (iii) the backward evolution from t_n to t_0, i.e., $|\psi_R(t_0)\rangle = U^\dagger(t_0, t_n)|\tilde{\psi}(t_n)\rangle$. The expectation value of the square of the momentum can then be calculated using $|\psi_R(t_0)\rangle$ to obtain $C_1(t_n)$ [see Eq. (4)]. To numerically simulate $C_2(t)$, the operator p should first be applied to the initial state $|\psi(t_0)\rangle$, yielding the new state $|\varphi(t_0)\rangle = p|\psi(t_0)\rangle$. Then, the forward evolution is conducted, i.e., $|\varphi(t_n)\rangle = U(t_0, t_n)|\varphi(t_0)\rangle$. Subsequently, the action of p is performed on $|\varphi(t_n)\rangle$, obtaining $|\tilde{\varphi}(t_n)\rangle = p|\varphi(t_n)\rangle$, afterwards, the time reversal is applied to $|\tilde{\varphi}(t_n)\rangle$, resulting in $|\varphi_R(t_0)\rangle = U^\dagger(t_0, t_n)|\tilde{\varphi}(t_n)\rangle$. Using Eq. (5), $C_2(t_n)$ can then be calculated by evaluating the norm of $|\varphi_R(t_0)\rangle$. Lastly, the term $C_3(t_n)$ [see Eq. (6)] can be determined using the two states $|\psi_R(t_0)\rangle$ and $|\varphi_R(t_0)\rangle$, which is usually complex since they are not identical.

In the $\mathcal{PT}$-symmetry breaking phase, the norm of the quantum state $\mathcal{N}_\psi(t_n) = \langle\psi(t_n)|\psi(t_n)\rangle$ increases exponentially with time regardless of the forward or backward evolution. To address this issue and eliminate its contribution to the OTOCs, we normalize the time-evolved state. For the forward evolution $t_0 \rightarrow t_n$ of $|\psi(t_0)\rangle$, we set the norm of the quantum state to be the same as that of the initial state, i.e., $\mathcal{N}_\psi(t_j) = \langle\psi(t_0)|\psi(t_0)\rangle$ with $0 \leqslant j \leqslant n$. The backward evolution starts from the state $|\tilde{\psi}(t_n)\rangle$ whose norm $\mathcal{N}_{\tilde{\psi}}(t_n) = \langle\psi(t_n)|p^2|\psi(t_n)\rangle$ is the mean energy of the state $|\psi(t_n)\rangle$. Thus, it is reasonable to take the norm of the quantum state during the backward evolution $t_n \rightarrow t_0$ to be $\mathcal{N}_{\tilde{\psi}}(t_n)$, i.e., $\mathcal{N}_{\psi_R}(t_j) = \mathcal{N}_{\tilde{\psi}}(t_n)$. In short, the norm of the time-evolved state for both the forward and backward evolution is equal to that of the state it starts from. If the same normalization procedure is applied to the evolution of $|\varphi(t_n)\rangle$, then we will have $\mathcal{N}_\varphi(t_j) = \langle\varphi(t_0)|\varphi(t_0)\rangle$ and $\mathcal{N}_{\varphi_R}(t_j) = \langle\tilde{\varphi}(t_n)|\tilde{\varphi}(t_n)\rangle$ $(0 \leqslant j \leqslant n)$ for the forward and time reversal evolutions, respectively.

To understand the effects of $\mathcal{PT}$-symmetry breaking on the dynamics of $C(t_n)$, we numerically investigate the time evolution of $C(t_n)$ for different λ. Figure 2(a) shows that, for values of λ smaller than the phase transition point (e.g., $\lambda = 10^{-5} \ll \lambda_c$), the $C(t_n)$ increases gradually up to saturation. Interestingly, for λ slightly larger than λ_c, the $C(t_n)$ increases in a power-law of time, i.e., $C(t_n) \propto t^\eta$ with $\eta > 2$ [see $\lambda = 0.022$
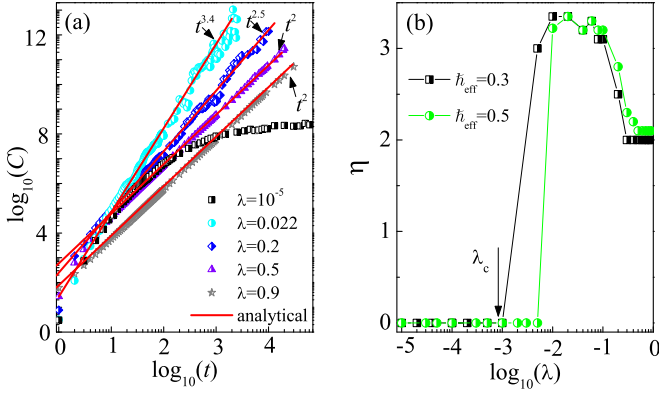
FIG. 2. (a) Time dependence of C for $K = 6$ with $\lambda = 10^{-5}$ (squares), 0.022 (circles), 0.2 (diamonds), 0.5 (triangles), and 0.9 (pentagrams). Solid lines in red denote theoretical prediction in Eqs. (12) and (13), i.e., $C(t) \propto t^{\eta}$. (b) The η versus λ for $\hbar_{\mathrm{eff}} = 0.3$ (squares) and 0.5 (circles). Arrow marks the phase transition point $\lambda_c \approx 0.001$ for $\hbar_{\mathrm{eff}} = 0.3$.

with $\eta = 3.4$ in Fig. 2(a)]. We dub this phenomenon as a superquadratic growth (SQG) of $C(t_n)$. When the value of λ is much larger than the phase transition point, i.e., $\lambda \gg \lambda_c$ [e.g., $\lambda = 0.5$ and 0.9 in Fig. 2(a)], the quadratic growth (QG) of OTOCs $C(t_n) \propto t^2$ emerges. We further investigate the exponent η for different λ. Our results show that η is 0 for $\lambda < \lambda_c$, increases abruptly to a maximum value greater than 2 for λ slightly larger than λ_c, and finally saturates to 2 for sufficiently large λ [e.g., see $\hbar_{\mathrm{eff}} = 0.3$ in Fig. 2(b)]. It is evident that the scaling law of OTOCs reveals the emergence of the spontaneous $\mathcal{PT}$-symmetry breaking and unveils the correlation between information scrambling and the $\mathcal{PT}$-symmetry phase transition.

IV. THEORETICAL ANALYSIS OF THE DYNAMICS OF OTOCs

A. Mechanism of the saturation of $C(t)$ for $\lambda < \lambda_c$

We numerically investigate the time evolution of the three parts of the OTOCs, i.e., C_1, C_2, and C_3 for $\lambda < \lambda_c$. Figure 3(a) shows that the time dependence of C_1 and C almost overlap, displaying rapid growth up to saturation. Since the real part of C_3, i.e., $\mathrm{Re}(C_3)$ fluctuates between positive and negative values, we plot the absolute value $|\mathrm{Re}(C_3)|$ in Fig. 3(b). Both C_2 and $|\mathrm{Re}[C_3]|$ saturate after a very short time evolution. Importantly, C_1 is at least four orders of magnitude larger than both C_2 and $|\mathrm{Re}[C_3]|$, leading to a perfect consistency between C_1 and C. Consequently, based on Eq. (3), we can safely use the approximation

$$C(t_n) \approx \langle \psi_R(t_0)|p^2|\psi_R(t_0)\rangle = \langle p^2(t_0)\rangle_R \mathcal{N}_{\psi_R}(t_0), \quad (7)$$

where $\langle p^2(t_0)\rangle_R = \langle \psi_R(t_0)|p^2|\psi_R(t_0)\rangle / \mathcal{N}_{\psi_R}(t_0)$ denotes the expectation value of energy of the state $|\psi_R(t_0)\rangle$ divided by its norm $\mathcal{N}_{\psi_R}(t_0) = \langle \psi_R(t_0)|\psi_R(t_0)\rangle$.

The normalization procedure for time reversal yields the equivalence $\mathcal{N}_{\psi_R}(t_0) = \mathcal{N}_{\tilde{\psi}}(t_n) = \langle \psi(t_n)|p^2|\psi(t_n)\rangle$, which shows that the value of $\mathcal{N}_{\psi_R}(t_0)$ is just the mean energy of the state $|\psi(t_n)\rangle$ at the time $t = t_n$. For $\lambda < \lambda_c$, the quasienergies are all real, thus the dynamics of the PTKR is the same
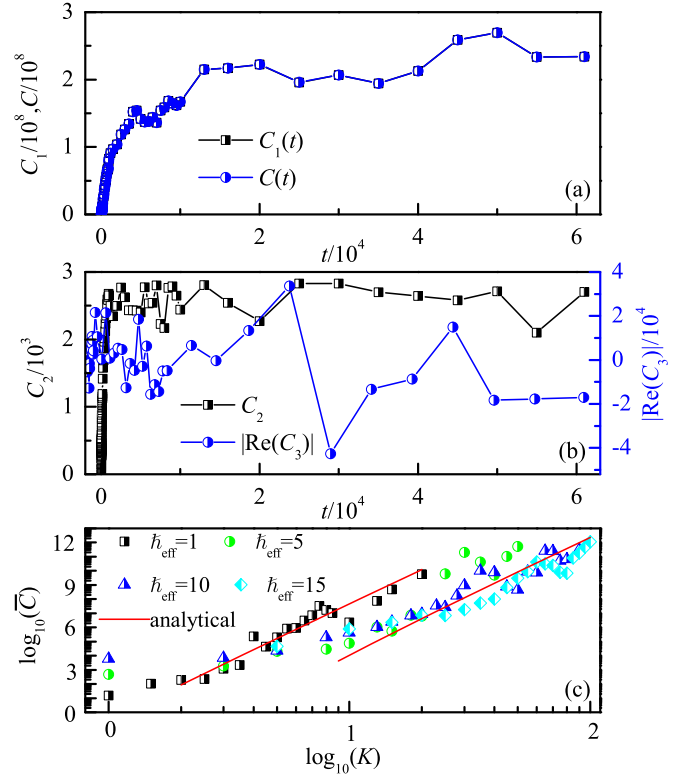

FIG. 3. (a) Time evolution of C (circles) and C_1 (squares). Note that C almost fully overlaps with C_1. (b) Dependence of C_2 (squares) and $|\mathrm{Re}(C_3)|$ (circles) on time. The parameters are $K = 6$, $\lambda = 10^{-5}$, and $\hbar_{\mathrm{eff}} = 0.3$. (c) The $\bar{C}$ versus K with $\lambda = 10^{-5}$ for $\hbar_{\mathrm{eff}} = 1$ (squares), 5 (circles), 10 (triangles), and 15 (diamonds). Solid lines indicate our theoretical prediction in Eq. (8).

as that of the Hermitian QKR. A noteworthy characteristic of the QKR's energy diffusion is the phenomenon of DL, i.e., the mean energy $\langle p^2 \rangle$ gradually approaches to saturation level with increasing time due to quantum coherence. It is reasonable to believe that the mechanism of DL suppresses the growth of both $\mathcal{N}_{\psi_R}(t_0)$ and $\langle p^2(t_0)\rangle_R$, and therefore leads to the saturation of $C(t_n)$.

To confirm this conjecture, we consider a specific time, i.e., $t = t_n$, and numerically trace the evolution of $\langle p^2 \rangle$ for both the forward ($t < t_n$) and backward ($t > t_n$) evolution. Figure 4(a) shows that for $t_n = 2500$, $\langle p^2 \rangle$ increases rapidly to saturation during forward time evolution from t_0 to t_{2500}, then jumps to a specific value at the start of the time reversal (i.e., at $t = t_{2500}$) before finally saturating for the backward evolution from t_{2500} to t_0. This clearly demonstrates the emergence of the DL, which is also reflected by the probability density distribution in momentum space. We compare the momentum distributions at the end of the forward evolution (i.e., $t = t_{2500}$) and the end of time reversal (i.e., $t = t_0$) in Fig. 4(b). One can see that the two quantum states almost overlap with each other, both of which are exponentially localized in momentum space, i.e., $|\psi(t_n)|^2 \sim \exp(-|p|/L)$ [see Fig. 4(b)]. A rough estimation yields $\mathcal{N}_{\psi_R}(t_0) = \langle \psi(t_n)|p^2|\psi(t_n)\rangle \sim L^2$ and $\langle p^2(t_0)\rangle_R \sim \int_{-\infty}^{\infty} p^2 \exp(-|p|/L)dp \sim L^2$. Plugging the two relations into Eq. (7), we can immediately obtain the estimation of the OTOCs, i.e., $C(t_n) \sim L^4$. It is known that the
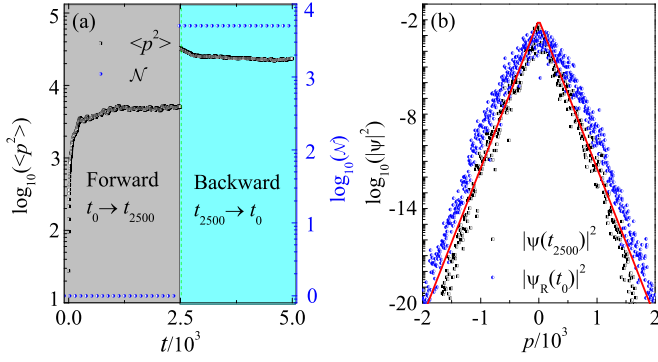
FIG. 4. (a) Time trace of $\langle p^2 \rangle$ (squares) and $\mathcal{N}$ (circles) during the forward evolution $t_0 \rightarrow t_{2500}$, the action of p at the time $t = t_{2500}$, and the time reversal $t_{2500} \rightarrow t_{5000}$. Green dashed line marks $t_n = 2500$. (b) Momentum distributions for the state $|\psi(t)\rangle$ (squares) at the time $t_n = 2500$ and the state $|\psi_R(t_0)\rangle$ (circles) at the end of time reversal. Solid line indicates the exponentially localized shape $|\psi(p)|^2 \propto e^{-|p|/L}$ with $L \approx 46$. The parameters are $K = 6$, $\lambda = 10^{-5}$, and $\hbar_{\text{eff}} = 0.3$.

localization length is in a quadratic function of K, i.e., $L \propto K^2$ [103], which results in the relation

$$C \propto K^8. \tag{8}$$

This clearly demonstrates that the C is time independent after the long term evolution, verifying our numerical results in Figs. 2(a) and 3(a).

To provide evidence of our analytical prediction, we investigate the time-averaged value of OTOCs, i.e., $\bar{C} = \sum_{j=1}^{N} C(t_j)/N$, numerically for different K. In the numerical simulations, we ensure that N is large enough for the long-term saturation of $C(t)$ to be well quantified by $\bar{C}$. Our numerical results show that, for a specific $\hbar$, $\bar{C}$ increases in a power law of K [see Fig. 3(c)], which is well described by our theoretical prediction in Eq. (8). This is a strong indication of the validity of our analytical analysis. Our findings of the dependence of the OTOCs on the kick strength provide an opportunity to control the operator growth with an external driven potential.

The discontinuous jump in the mean square momentum, $\langle p^2 \rangle$, at $t = t_{2500}$, the beginning of time reversal, is due to the action of the operator p on the quantum state $|\psi(t_{2500})\rangle$. This action generates the quantum state $|\tilde{\psi}(t_{2500})\rangle = p|\psi(t_{2500})\rangle$, for which the mean value is given by $\langle \tilde{\psi}(t_{2500})|p^2|\tilde{\psi}(t_{2500})\rangle = \langle \psi(t_{2500})|p^4|\psi(t_{2500})\rangle$. The exponentially localized shape of the quantum state $|\psi(t_{2500})|^2 \sim \exp(-|p|/L)$ [see Fig. 4(b)] allows us to obtain the expectation values $\langle \psi(t_{2500})|p^2|\psi(t_{2500})\rangle \sim L^2 \hbar_{\text{eff}}^2$ and $\langle \tilde{\psi}(t_{2500})|p^2|\tilde{\psi}(t_{2500})\rangle = \langle \psi(t_{2500})|p^4|\psi(t_{2500})\rangle \sim L^4 \hbar_{\text{eff}}^4$, which quantitatively explains the discontinuous increase in the mean energy from $L^2 \hbar_{\text{eff}}^2$ to $L^4 \hbar_{\text{eff}}^4$.

In the PTKR model, the DL takes place in the unbroken phase of $\mathcal{PT}$-symmetry, where the strength of the imaginary component of the kicking potential is smaller than a specific threshold value. In this phase, the DL mechanism is identical to that of the Hermitian QKR model since the quasienergies are real. The manifestation of DL is distinctly illustrated by the time evolution of the mean energy, as depicted in Fig. 4.
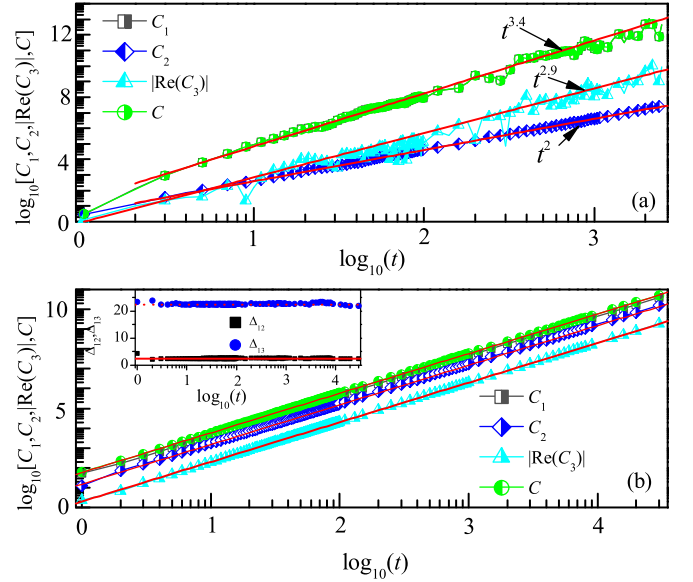

FIG. 5. Time evolution of C_1 (squares), C_2 (diamonds), $|\text{Re}(C_3)|$ (triangles), and C (circles) for $\lambda =$ (a) 0.022 and (b) 0.9. In (a) the red lines indicate the power-law fitting. In (b) the red lines indicate the quadratic function $C_1 \approx 44t^2$, $C_2 \approx 17t^2$, and $|\text{Re}(C_3)| \approx 2t^2$. Inset: The Δ_{12} (squares) and Δ_{13} (circles) versus time. Solid (dashed-dotted) line denotes $\Delta_{12} \approx 2.5$ ($\Delta_{13} \approx 22$). Other parameters are the same as that in Fig. 4.

Our analysis of the time evolution of the OTOCs for $\lambda < \lambda_c$ reveals that the DL mechanism contributes to the saturation of OTOCs (see Fig. 3). We investigate the quantum diffusion in a non-Hermitian QKR model, utilizing a form of non-Hermitian driven potential $V(\theta) = (K + i\lambda)\cos(\theta)$ [47]. The energy diffusion of this system displays an interesting DL, characterized by a decrease of the saturation of mean energy with the increase of the non-Hermitian parameter λ. Thus, it is evident that the non-Hermitian kicking potential can actually amplify the degree of DL in comparison to the Hermitian QKR model. By extending the Floquet theory to non-Hermitian cases, we predict that the quantum state will ultimately evolve into a quasieigenstate with a predominantly large imaginary part of the quasienergy. The localization of this state dictates the DL of a time-evolved state [47,104], which differs from the mechanism of DL in the Hermitian QKR model [77–80].

B. Mechanism of the SQG of $C(t)$ for $\lambda \gtrsim \lambda_c$

Figure 5(a) shows the time evolution of C_1, C_2, $|\text{Re}(C_3)|$, and C for λ just larger than the $\mathcal{PT}$-symmetry phase transition point $\lambda \gtrsim \lambda_c$. It is clear that the time dependence of C_1 corresponds perfectly to that of C, both of which increase following the SQG $C \propto t^{3.4}$. The time evolution of C_2 displays the QG, i.e., $C_2(t) \propto t^2$, while $|\text{Re}(C_3)|$ follows the SQG $|\text{Re}(C_3)| \sim t^{2.9}$. In addition, one can see that C_1 is larger than both C_2 and $|\text{Re}(C_3)|$ by approximately four orders of magnitude. Therefore, it is sufficient to analyze the time evolution of the term C_1 to uncover the mechanism of the SQG of C.

Since the value of $C(t)$ at a specific time $t = t_n$ is dependent on both the mean energy $\langle p^2(t_0)\rangle_R$ and the norm
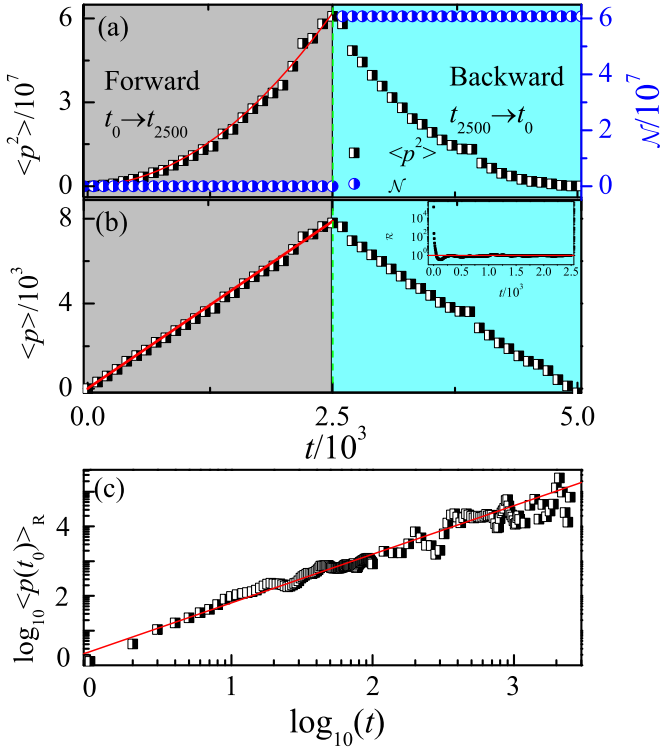
FIG. 6. Top two panels: Time trace of $\langle p^2 \rangle$ (squares) in (a), $\mathcal{N}$ (circles) in (a), and $\langle p \rangle$ in (b) during the forward evolution $t_0 \rightarrow t_{2500}$, the action of p at the time $t = t_{2500}$, and the time reversal $t_{2500} \rightarrow t_{5000}$. Green dashed lines mark $t = t_{2500}$. In (a) the red line indicates the quadratic function $\langle p^2 \rangle = \gamma^2 t^2$ with $\gamma \approx 3.2$. In (b) the red line indicates the linear growth $\langle p \rangle = \gamma t$. Inset: $\mathcal{R}$ versus time. Red line marks $\mathcal{R} = 1$. In (c) the time dependence of $\langle p^2(t_0) \rangle_R$. Red line indicates the power-law fitting $\langle p^2(t_0) \rangle_R \propto t^{1.4}$. The parameter is $\lambda = 0.022$. Other parameters are the same as Fig. 4.

$\mathcal{N}_{\psi_R}(t_0)$ of the state $|\psi_R(t_0)\rangle$ at the end of time reversal [see Eq. (7)], we numerically calculate the forward and backward time evolution of $\langle p^2 \rangle$, $\langle p \rangle$, and $\mathcal{N}$ with a fixed t_n (e.g., $t_n = 2500$ in Fig. 6). Figure 6(a) demonstrates that the mean energy diffuses ballistically with time $\langle p^2 \rangle \approx \gamma^2 t^2$ during the forward evolution $t_0 \rightarrow t_{2500}$ and it displays the intrinsic time reversal during $t_{2500} \rightarrow t_0$. Meanwhile, the mean momentum $\langle p \rangle$ linearly increases for $t_0 < t < t_{2500}$, and linearly decays for $t_{2500} \rightarrow t_0$ [see Fig. 6(b)]. Moreover, Fig. 6(a) reveals that the norm remains unity, i.e., $\mathcal{N}(t) = 1$, during the forward evolution and equals the mean energy at the time $t = t_{2500}$, i.e., $\mathcal{N}_{\psi_R}(t_j) = \langle p^2(t_{2500}) \rangle$ during the time reversal. Taking the ballistic diffusion of energy into account, the following equivalence can be derived

$$\mathcal{N}_{\psi_R}(t_0) = \gamma^2 t_n^2. \quad (9)$$

To measure the degree of time reversal for a fixed t_n, we define the ratio of mean energy between forward ($t < t_n$) and backward ($t > t_n$) time evolution as

$$\mathcal{R}(t_j) = \frac{\langle p^2(2t_n - t_j) \rangle_R}{\langle p^2(t_j) \rangle}, \quad (10)$$

where $\langle p^2(t_j) \rangle$ and $\langle p^2(2t_n - t_j) \rangle_R$ ($0 \leqslant j \leqslant n$) denote the mean square of momentum for the forward evolution and time
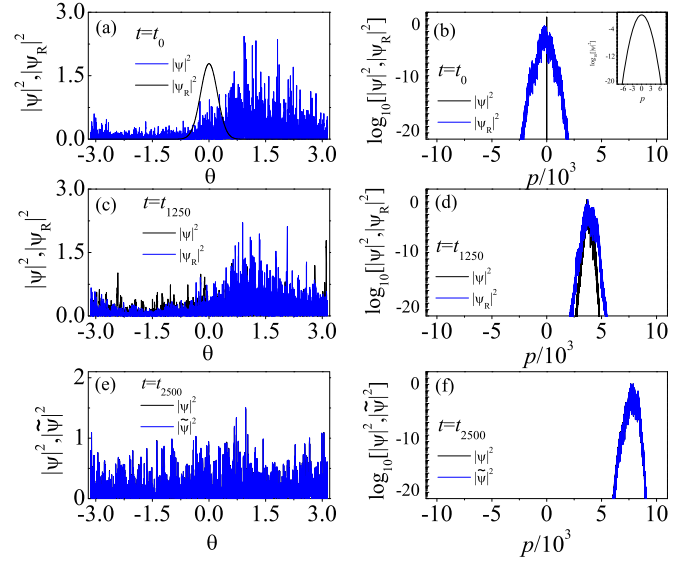

FIG. 7. Probability density distributions in real (left panels) and momentum (right panels) space for $\lambda = 0.022$. (a)–(d) Black and blue lines separately correspond to the states at forward $|\psi(t)\rangle$ and backward $|\psi_R(t)\rangle$ evolution with $t = t_0$ (top panels) and $t = t_{1250}$ (middle panels). Inset in (b) shows a magnified view of the momentum distribution for the initial Gaussian wavepacket around $p = 0$. Bottom panels: Probability density distributions in real (e) and momentum (f) space at the time $t = t_{2500}$. Black and blue lines indicate the state $|\psi(t_{2500})\rangle$ and $|\tilde{\psi}(t_{2500})\rangle = p|\psi(t_{2500})\rangle$, respectively. Other parameters are the same as Fig. 4.

reversal, respectively. The inset in Fig. 6(b) shows that $\mathcal{R}$ is very large (i.e., $\mathcal{R} \gtrsim 10^4$ for $t = t_0$) and approaches almost 1 with time evolution. This reveals that the mean energy at the end of time reversal is much greater than that at the initial time, i.e., $\langle p^2(t_0) \rangle_R \gg \langle p^2(t_0) \rangle$. We further investigate the time evolution of $\langle p^2(t_0) \rangle_R$, and find [see Fig. 6(c)] that the $\langle p^2(t_0) \rangle_R$ increases in the power law of time

$$\langle p^2(t_0) \rangle_R \propto t^{1.4}. \quad (11)$$

Substituting Eqs. (9) and (11) into Eq. (7) yields the SQG of OTOCs

$$C(t) \propto t^\eta \quad \text{with} \quad \eta \approx 3.4. \quad (12)$$

Figure 7 shows the probability density distribution of the state at forward $|\psi(t_j)\rangle$ and backward $|\psi_R(t_j)\rangle$ evolution in both the real and momentum space. The initial state is a Gaussian wavepacket $\psi(\theta, t_0) = (\sigma/\pi)^{1/4} \exp(-\sigma\theta^2/2)$ centered at $\theta = 0$ and $p = 0$ [see Figs. 7(a) and 7(b)]. Interestingly, one can observe that the quantum state is mainly distributed in the region $0 < \theta < \pi$ for both the forward and backward evolution. This is due to the fact that the action of the Floquet operator of the kicking term $U_K(\theta) = \exp[K\lambda \sin(\theta)/\hbar_{\text{eff}}] \exp[-iK \cos(\theta)/\hbar_{\text{eff}}]$ on a quantum state, i.e., $U_K(\theta)\psi(\theta)$ helps to amplify the state within the region $0 < \theta < \pi$ as $K\lambda \sin(\theta) > 0$. Assuming that the real part of the kicking potential provides the driven force $F = K \sin(\theta)$, the PTKR experiences a positive magnitude force $F > 0$ during the forward evolution, thus the momentum grows with time, as shown in Fig. 6(b). For the time reversal, the sign of
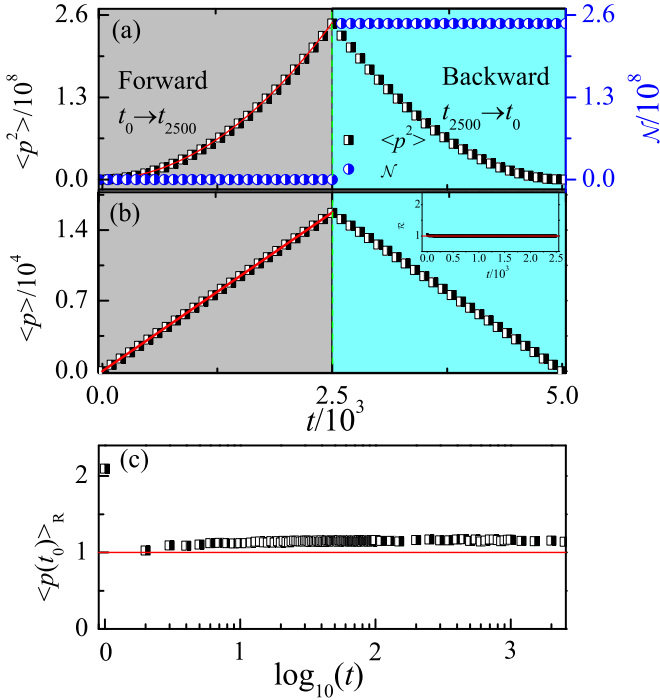
FIG. 8. Same as in Fig. 6 but for $\lambda = 0.9$. In (a) the red line indicates the quadratic function $\langle p^2 \rangle = \gamma^2 t^2$ with $\gamma \approx 6.3$. In (b) the red line denotes the linear growth $\langle p \rangle = \gamma t$. In (c) the red line indicates $\langle p(t_0) \rangle_R \approx 1$.

kick strength K flips, i.e., $K \to -K$, so the mean momentum decreases with time evolution. Our conjecture is supported by the numerical results of momentum distributions. Figures 7(b), 7(d) and 7(f) show that the wavepacket, like a soliton, moves to the positive direction in momentum space for $t_0 \to t_{2500}$, resulting in $\langle p \rangle = \gamma t$ [in Fig. 6(b)], and moves back to the opposite direction for $t_{2500} \to t_0$. In addition, the width of the wavepacket in momentum space is so narrow that one can safely use the approximation $\langle p^2 \rangle \sim (\langle p \rangle)^2$, which is verified by our numerical results in Figs. 6(a).

C. Mechanism of the QG of $C(t)$ for $\lambda \gg \lambda_c$

We numerically investigate the time evolution of C_1, C_2, C_3, and C for $\lambda \gg \lambda_c$. As shown in Fig. 5(b), all of them increase in the way of QG (i.e., $\propto t^2$). We use the ratios $\Delta_{12} = C_1/C_2$ and $\Delta_{13} = C_1/|\text{Re}[C_3]|$ to quantify the differences among C_1, C_2, and $|\text{Re}[C_3]|$. Our investigation shows that both of them are larger than 1, specifically $\Delta_{12} \approx 2.5$ and $\Delta_{13} \approx 22$ [see the inset in Fig. 5]. This suggests that C_1 contributes mainly to the C, which is verified by the good agreement between C_1 and C [see Fig. 5(b)]. To reveal the mechanism of the QG of C, we proceed to analyze the time evolution of C_1 by thoroughly investigating both the forward and backward evolution of the mean values $\langle p^2 \rangle$, $\langle p \rangle$, and the norm $\mathcal{N}$ for a given t_n.

Figure 8(a) shows that the mean energy exhibits ballistic diffusion $\langle p^2 \rangle \approx \gamma^2 t^2$ during the forward evolution from t_0 to t_n and decays as the inverse of a quadratic function, with $\langle p^2 \rangle \propto t^{-2}$, during the backward evolution from t_n to t_0. This decay is symmetric with respect to the $\langle p^2 \rangle$ of $t < t_n$. The dynamics of the mean momentum also exhibits perfect
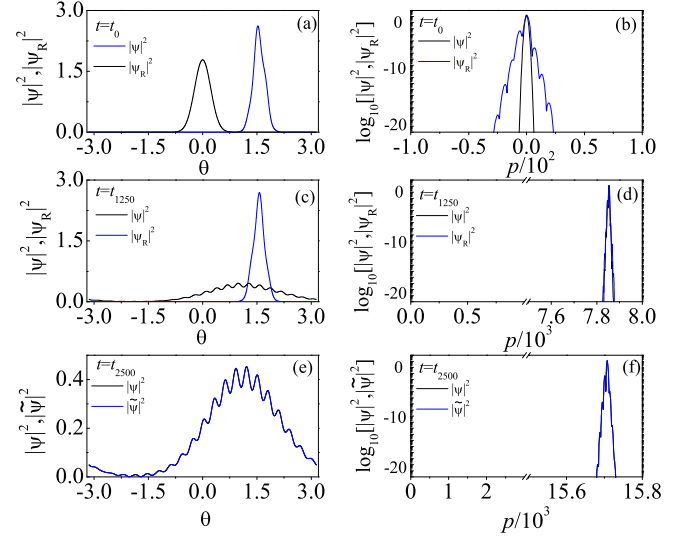

FIG. 9. Same as in Fig. 7 but for $\lambda = 0.9$.

time reversal, namely, it linearly increases as $\langle p \rangle = \gamma t$ during $t_0 \to t_{2500}$ and decreases linearly during $t_{2500} \to t_0$. The ratio $\mathcal{R}$ remains close to 1 throughout the time evolution, except at the end, i.e., $\mathcal{R}(t = 2500) \approx 2.5$ [see the inset in Fig. 8(b)], providing a clear evidence of time reversal. For the forward evolution from t_0 to t_{2500}, the norm $\mathcal{N}(t_j)$ is equal to unity, while for the interval $t_{2500} \to t_0$, it is equal to the value of $\langle p^2(t_{2500}) \rangle$, i.e., $\mathcal{N}_{\psi_R}(t_j) = \langle p^2(t_{2500}) \rangle$ [see Fig. 8(a)]. By utilizing the ballistic diffusion of mean energy, we establish the relationship $\mathcal{N}_{\psi_R}(t_0) \approx \mathcal{N}_{\psi_R}(t_n) \approx \gamma^2 t_n^2$, where t_n is an arbitrary time. We further evaluate the behavior of $\langle p^2(t_0) \rangle_R$ for different t_n. As shown in Fig. 8(c), the $\langle p^2(t_0) \rangle_R$ remains almost constant at a value of 1, indicating that it is independent of time. Plugging in the values of $\mathcal{N}_{\psi_R}(t_0)$ and $\langle p^2(t_0) \rangle_R$ into Eq. (7), we obtain the QG of OTOCs

$$C(t) \approx \gamma^2 t^{\eta} \quad \text{with} \quad \eta = 2. \tag{13}$$

The time reversal of a wavepacket's dynamics is clearly seen in the evolution of its momentum distributions. For the forward time evolution, the quantum state is localized at the point $\theta_c = \pi/2$ [see Figs. 9(a), 9(c) and 9(e)], which is the result of the localization effect of the imaginary part of the Floquet operator $U_K(\theta)$. With the wavepacket mimicking a classical particle, it experiences a kicking force of magnitude $F = K \sin(\theta_c) = K$, resulting in a constant acceleration of momentum $\Delta p = K$, which is reflected in the linear growth of momentum. This phenomenon of the directed current is also seen in the propagation of momentum distributions in Figs. 9(b), 9(d) and 9(f), where a soliton can be observed moving unidirectionally towards the positive direction in momentum space.

During the backward evolution, the wavepacket of the real space remains centered at $\theta_c = \pi/2$, with a width much smaller than the corresponding state at the time of forward evolution [see Figs. 9(a), 9(c) and 9(e)]. As the particle is exposed to the kicking force with $F = -K$ during time reversal, its momentum decreases linearly in time, which is also reflected in the propagation of the wavepackets in momentum space [Figs. 9(b), 9(d) and 9(f)]. It is evident that the $|\psi(t_n)|^2$

is in perfect overlap with the $|\psi_R(t_n)|^2$, apart from the initial state [see Fig. 9(b)]. The width of $|\psi_R(t_0)|^2$ is considerably larger than that of $|\psi(t_0)|^2$, leading to the ratio of energy being larger than one, i.e., $\mathcal{R} = \langle p^2(t_{5000})\rangle_R / \langle p^2(t_0)\rangle \approx 2.5$ [see the inset in Fig. 8(b)].

Our numerical findings clearly demonstrate that the probability density distribution of the PTKR model in angular coordinate space can unveil the signature of spontaneous $\mathcal{PT}$-symmetry breaking. In the $\mathcal{PT}$-symmetry phase, i.e., $\lambda < \lambda_c$, the quantum state is homogeneously distributed throughout the angular space. However, just beyond the phase transition points, i.e., $\lambda \gtrsim \lambda_c$, the quantum state primarily populates the region where $0 < \theta < \pi$ [see Figs. 7(a) and 7(c)]. As λ increases significantly beyond λ_c, the quantum state exhibits a well-localized shape around the point $\theta_c = \pi/2$ [see Figs. 9(a), 9(c) and 9(e)]. This localization results from the amplification of the probability density by the Floquet operator of the imaginary part of the kicking potential $U_K^R = \exp[K\lambda \sin(\theta)/\hbar_{\text{eff}}]$.

V. CONCLUSION AND DISCUSSION

In this work, we investigate the dynamics of OTOCs in a PTKR model and achieve its scaling laws in different phases of $\mathcal{PT}$ symmetry. We use the time series of the norm to train a LSTM, which enables us to extract a clear phase diagram of $\mathcal{PT}$-symmetry breaking, with a phase boundary at λ_c. For $\lambda < \lambda_c$, we find that the DL of energy diffusion suppresses the growth of OTOCs and prove analytically the dependence of OTOCs on the kicking strength, i.e., $C \propto K^8$. At the vicinity of the phase transition points, i.e., $\lambda \gtrsim \lambda_c$, we observe a SQG of OTOCs, i.e., $C(t) \propto t^\eta$ with an exponent $\eta > 2$. Interestingly, a QG of OTOCs, i.e., $C(t) \propto t^2$ emerges for $\lambda \gg \lambda_c$. We elucidate the mechanisms of both the SQG and QG by analyzing the time-reversed wavepacket's dynamics. Our results demonstrate that the spontaneous $\mathcal{PT}$-symmetry breaking profoundly affects the dynamics of OTOCs, providing an unprecedented opportunity for diagnosing the spontaneous $\mathcal{PT}$-symmetry breaking with OTOCs.

It has been proven that the long-term periodical driving can trigger the development of a thermal state with infinite temperature in interacting spin chains [100]. The prethermalization state in a paradigm model of many-body chaos, i.e., interacting kicked rotors, can be effectively characterized by a generalized Gibbs ensemble with a well-defined temperature [77]. The features of prethermalization, crossover regime, and heating phases can be identified through the spatiotemporal fluctuation correlation of kinetic energy [78]. For the PTKR, the mean energy increases unboundedly in condition that $\lambda > \lambda_c$, suggesting a rise in temperature towards infinity. Our theoretical analysis indicates that the quantum diffusion of energy underlies the power-law growth of OTOCs, thereby linking quantum heating and quantum scrambling. The intrinsic relationship between quantum diffusion, quantum thermalization, and quantum scrambling is a fundamental issue that has garnered significant attention, particularly for non-Hermitian systems in recent years. Our discovery of diffusion-induced scaling laws for OTOCs presents a different aspect in this fascinating field and enriches our understanding of the
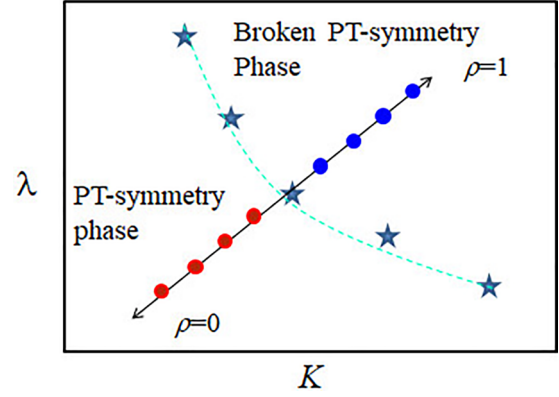

FIG. 10. Schematic diagram illustrates the method for training the LSTM network. Pentagrams indicate the phase transition points λ_c, which approximately outline the phase boundary (green dashed line). Double-ended arrow line denotes a series of discrete parameters (λ_j, K_j) with $1 \leqslant j \leqslant N$, in which red and blue circles are characterized by $\rho = 0$ and 1, respectively.

fundamental problems associated with the quantum-classical transition in non-Hermitian chaotic systems [104,105].

In recent years, the OTOCs were widely used to investigate the operator growth in quantum mapping systems [106], the information scrambling in spin chains [107], and the quantum thermalization in many-body chaotic systems [108]. Theoretical studies demonstrated that the QKR model is mathematically equivalent to the kicked Heisenberg spin XXZ chain [109], indicating a connection between the magnon dynamics and quantum diffusion of chaotic systems. Our findings therefore bridge the gap between the information scrambling in condensed matter physics and the operator growth in quantum chaotic systems. This also paves the way for the experimental observation of OTOCs dynamics in chaotic systems using spin chain platforms. Based on the equivalence between the light propagation equation under paraxial approximation and the Schrödinger equation, the author of Ref. [49] proposed an optical setup composed of a Fabry-Perot resonator with flat end mirrors and combined thin index and loss gratings to emulate the wavepacket dynamics of the PTKR model. The reflection of light by the mirrors simulates the delta kicking, while the combined thin index and loss gratings assume the role of the $\mathcal{PT}$-symmetric potential. The quantum ratchet transport of optics is observed in the frequency domain. Therefore, our findings could be realized using state-of-the-art experimental techniques.

APPENDIX: DETAILS OF THE LSTM METHOD

Figure 10 shows the schematic strategy for training the long short-term memory (LSTM) network. There are three steps.

(i) First, we numerically search several phase transition points λ_c based the dependence of time-averaged $\bar{\mathcal{N}}$ on λ [see Fig. 1(b)], which allows us to outline approximately the phase boundary [see the dashed line in Fig. 10].

(ii) Second, we sketch a straight line that is approximately perpendicular, intersecting the midpoint of the phase boundary. Along this line, we select hundreds of discrete parameter values for (λ_j, K_j) with $1 \leqslant j \leqslant N$ and numerically calculate the corresponding time evolution of the norm $\mathcal{N}_j(t)$. Note that the norm of the parameters below (above) the phase boundary exhibits a characteristic value of $\rho = 0$ ($\rho = 1$), indicative of the $\mathcal{PT}$-symmetry (broken PT-symmetry) phase. We utilize the data $\mathcal{N}_j(t)$ to perform supervized training on the LSTM.

(iii) Finally, we numerically calculate the norm $\mathcal{N}(t)$ across a wide range of parameter values in the (λ, K) space. By inputting these time series of norms into the trained LSTM, we obtain the probability ρ, which determines whether the parameter (λ, K) is in the $\mathcal{PT}$-symmetry phase or not.

[1] H. Markum, R. Pullirsch, and T. Wettig, Non-Hermitian Random Matrix Theory and Lattice QCD with Chemical Potential, Phys. Rev. Lett. **83**, 484 (1999).

[2] N. Hatano and D. R. Nelson, Localization Transitions in Non-Hermitian Quantum Mechanics, Phys. Rev. Lett. **77**, 570 (1996).

[3] M. Berry, Physics of Nonhermitian Degeneracies, Czech. J. Phys. **54**, 1039 (2004).

[4] E. M. Graefe, H. J. Korsch, and A. E. Niederle, Mean-Field Dynamics of a Non-Hermitian Bose-Hubbard Dimer, Phys. Rev. Lett. **101**, 150408 (2008).

[5] I. Rotter, A non-Hermitian Hamilton operator and the physics of open quantum systems, J. Phys. A: Math. Theor. **42**, 153001 (2009).

[6] G. Barontini, R. Labouvie, F. Stubenrauch, A. Vogler, V. Guarrera, and H. Ott, Controlling the Dynamics of an Open Many-Body Quantum System with Localized Dissipation, Phys. Rev. Lett. **110**, 035302 (2013).

[7] K. Jones-Smith and H. Mathur, Relativistic Non-Hermitian Quantum Mechanics, Phys. Rev. D **89**, 125014 (2014).

[8] B. Ostahie and A. Aldea, Phosphorene confined systems in magnetic field, quantum transport, and superradiance in the quasiflat band, Phys. Rev. B **93**, 075408 (2016).

[9] Y. Ashida, Z. Gong, and M. Ueda, Non-hermitian physics, Adv. Phys. **69**, 249 (2020).

[10] C. Keller, M. K. Oberthaler, R. Abfalterer, S. Bernet, J. Schmiedmayer, and A. Zeilinger, Tailored Complex Potentials and Friedel's Law in Atom Optics, Phys. Rev. Lett. **79**, 3327 (1997).

[11] C. M. Bender and S. Boettcher, Real Spectra in Non-Hermitian Hamiltonians Having $\mathcal{PT}$ Symmetry, Phys. Rev. Lett. **80**, 5243 (1998).

[12] C. M. Bender, D. C. Brody, and H. F. Jones, Complex Extension of Quantum Mechanics, Phys. Rev. Lett. **89**, 270401 (2002).

[13] A. Mostafazadeh, Pseudo-Hermiticity versus PT-symmetry. II. A complete characterization of non-Hermitian Hamiltonians with a real spectrum, J. Math. Phys. **43**, 2814 (2002).

[14] C. M. Bender, Making sense of non-Hermitian Hamiltonians, Rep. Prog. Phys. **70**, 947 (2007).

[15] A. Mostafazadeh, Pseudo-hermitian representation of quantum mechanics, Int. J. Geom. Methods Mod. Phys. **07**, 1191 (2010).

[16] K. Jones-Smith and H. Mathur, Non-Hermitian quantum Hamiltonians with $\mathcal{PT}$ symmetry, Phys. Rev. A **82**, 042101 (2010).

[17] R. El-Ganainy, K. G. Makris, M. Khajavikhan, Z. H. Musslimani, S. Rotter, and D. N. Christodoulides, Non-Hermitian physics and PT symmetry, Nat. Phys. **14**, 11 (2018).

[18] S. Klaiman, U. Günther, and N. Moiseyev, Visualization of Branch Points in PT-Symmetric Waveguides, Phys. Rev. Lett. **101**, 080402 (2008).

[19] Z. H. Musslimani, K. G. Makris, R. El-Ganainy, and D. N. Christodoulides, Optical Solitons in PT Periodic Potentials, Phys. Rev. Lett. **100**, 030402 (2008).

[20] Y. Chu, Y. Liu, H. Liu, and J. Cai, Quantum Sensing with a Single-Qubit Pseudo-Hermitian System, Phys. Rev. Lett. **124**, 020501 (2020).

[21] E. J. Bergholtz, J. C. Budich, and F. K. Kunst, Exceptional topology of non-Hermitian systems, Rev. Mod. Phys. **93**, 015005 (2021).

[22] S. Yao and Z. Wang, Edge States and Topological Invariants of Non-Hermitian Systems, Phys. Rev. Lett. **121**, 086803 (2018).

[23] X. M. Zhao, C. X. Guo, M. L. Yang, H. Wang, W. M. Liu, and S. P. Kou, Anomalous non-Abelian statistics for non-Hermitian generalization of Majorana zero modes, Phys. Rev. B **104**, 214502 (2021).

[24] Z. F. Yu, J. K. Xue, L. Zhuang, J. Zhao, and W. M. Liu, Non-Hermitian spectrum and multistability in exciton-polariton condensates, Phys. Rev. B **104**, 235408 (2021).

[25] X. M. Zhao, C. X. Guo, S. P. Kou, L. Zhuang, and W. M. Liu, Defective Majorana zero modes in a non-Hermitian Kitaev chain, Phys. Rev. B **104**, 205131 (2021).

[26] F. Yu, X. L. Zhang, Z. N. Tian, Q. D. Chen, and H. B. Sun, General Rules Governing the Dynamical Encircling of an Arbitrary Number of Exceptional Points, Phys. Rev. Lett. **127**, 253901 (2021).

[27] W. Y. Wang, B. Sun, and J. Liu, Adiabaticity in nonreciprocal Landau-Zener tunneling, Phys. Rev. A **106**, 063708 (2022).

[28] Y. Huang, Y. Shen, C. Min, S. Fan, and G. Veronis, Unidirectional reflectionless light propagation at exceptional points, Nanophotonics **6**, 977 (2017).

[29] K. G. Zloshchastiev and A. Sergi, Comparison and unification of non-Hermitian and Lindblad approaches with applications to open quantum optical systems, J. Mod. Opt. **61**, 1298 (2014).

[30] K. G. Makris, R. El-Ganainy, D. N. Christodoulides, and Z. H. Musslimani, Beam Dynamics in PT Symmetric Optical Lattices, Phys. Rev. Lett. **100**, 103904 (2008).

[31] R. El-Ganainy, K. G. Makris, D. N. Christodoulides, and Z. H. Musslimani, Theory of coupled optical PT-symmetric structures, Opt. Lett. **32**, 2632 (2007).

[32] A. Guo, G. J. Salamo, D. Duchesne, R. Morandotti, M. Volatier-Ravat, V. Aimez, G. A. Siviloglou, and D. N. Christodoulides, Observation of PT-Symmetry Breaking in Complex Optical Potentials, Phys. Rev. Lett. **103**, 093902 (2009).

[33] A. Regensburger, C. Bersch, M.-A. Miri, G. Onishchukov, D. N. Christodoulides, and U. Peschel, Parity-time synthetic photonic lattices, Nature (London) **488**, 167 (2012).

[34] H. Hodaei, M. A. Miri, M. Heinrich, and M. Khajavikhan, Parity-time-symmetric microring lasers, Science **346**, 975 (2014).

[35] L. Feng, Z. J. Wong, R. M. Ma, Y. Wang, and X. Zhang, Single-mode laser by parity-time symmetry breaking, Science **346**, 972 (2014).

[36] J. Li, R. Yu, C. Ding, and Y. Wu, PT-symmetry-induced evolution of sharp asymmetric line shapes and high-sensitivity refractive index sensors in a three-cavity array, Phys. Rev. A **93**, 023814 (2016).

[37] S. Longhi, Bloch Oscillations in Complex Crystals with PT Symmetry, Phys. Rev. Lett. **103**, 123601 (2009).

[38] S. Longhi, Optical Realization of Relativistic Non-Hermitian Quantum Mechanics, Phys. Rev. Lett. **105**, 013903 (2010).

[39] C. E. Rüter, K. G. Makris, R. El-Ganainy, D. N. Christodoulides, M. Segev, and D. Kip, Observation of parity-time symmetry in optics, Nat. Phys. **6**, 192 (2010).

[40] Y. Xue, C. Hang, Y. He, Z. Bai, Y. Jiao, G. Huang, J. Zhao, and S. Jia, Experimental observation of partial parity-time symmetry and its phase transition with a laser-driven cesium atomic gas, Phys. Rev. A **105**, 053516 (2022).

[41] Q. Lin, T. Y. Li, K. K. Wang, W. Yi, and P. Xue, Observation of non-Hermitian topological Anderson insulator in quantum dynamics, Nat. Commun. **13**, 3229 (2022).

[42] L. Xiao, X. Zhan, Z. H. Bian, K. K. Wang, X. Zhang, X. P. Wang, J. Li, K. Mochizuki, D. Kim, N. Kawakami, W. Yi, H. Obuse, B. C. Sanders, and P. Xue, Observation of topological edge states in parity-time-symmetric quantum walks, Nat. Phys. **13**, 1117 (2017).

[43] A. Stegmaier, S. Imhof, and T. Helbig, Topological Defect Engineering and PT Symmetry in Non-Hermitian Electrical Circuits, Phys. Rev. Lett. **126**, 215302 (2021).

[44] X. Y. Lü, H. Jing, J. Y. Ma, and Y. Wu, PT-Symmetry-Breaking Chaos in Optomechanics, Phys. Rev. Lett. **114**, 253601 (2015).

[45] C. M. Bender, J. Feinberg, D. W. Hook *et al.*, Chaotic systems in complex phase space, Pramana **73**, 453 (2009).

[46] C. M. Bender, D. W. Hook, P. N. Meisinger, and Q. H. Wang, Complex Correspondence Principle, Phys. Rev. Lett. **104**, 061601 (2010).

[47] W. Zhao and H. Zhang, Dynamical stability in a non-Hermitian kicked rotor model, Symmetry **15**, 113 (2023).

[48] C. T. West, T. Kottos, and T. Prosen, PT-Symmetric Wave Chaos, Phys. Rev. Lett. **104**, 054102 (2010).

[49] S. Longhi, Localization, quantum resonances, and ratchet acceleration in a periodically kicked $\mathcal{PT}$-symmetric quantum rotator, Phys. Rev. A **95**, 012125 (2017).

[50] W. L. Zhao, J. Wang, X. Wang, and P. Tong, Directed momentum current induced by the PT-symmetric driving, Phys. Rev. E **99**, 042201 (2019).

[51] A. Larkin and Y. N. Ovchinnikov, Quasiclassical method in the theory of superconductivity, Sov. Phys. JETP **28**, 1200 (1969).

[52] D. A. Roberts, and B. Swingle, Lieb-Robinson Bound and the Butterfly Effect in Quantum Field Theories, Phys. Rev. Lett. **117**, 091602 (2016).

[53] J. Maldacena and D. Stanford, Remarks on the Sachdev-Ye-Kitaev model, Phys. Rev. D **94**, 106002 (2016).

[54] J. Polchinski and V. Rosenhaus, The spectrum in the Sachdev-Ye-Kitaev model, J. High Energy Phys. 04 (2016) 001.

[55] A. Bohrdt, C. Mendl, M. Endres, and M. Knap, Scrambling and thermalization in a diffusive quantum many-body system, New J. Phys. **19**, 063001 (2017).

[56] M. Gärttner, J. G. Bohnet, A. Safavi-Naini, M. L. Wall, J. J. Bollinger, and A. M. Rey, Measuring out-of-time-order correlations and multiple quantum spectra in a trapped-ion quantum magnet, Nat. Phys. **13**, 781 (2017).

[57] S. Banerjee and E. Altman, Solvable model for a dynamical quantum phase transition from fast to slow scrambling, Phys. Rev. B **95**, 134302 (2017).

[58] H. Shen, P. Zhang, R. Fan, and H. Zhai, Out-of-time-order correlation at a quantum phase transition, Phys. Rev. B **96**, 054503 (2017).

[59] R. Fan, P. Zhang, H. Shen, and H. Zhai, Out-of-time-order correlation for many-body localization, Sci. Bull. **62**, 707 (2017).

[60] Y. Huang, Y.-L. Zhang, and X. Chen, Out-of-Time- Ordered Correlators in Many-Body Localized Systems, Ann. Phys. (Leipzig) **529**, 1600318 (2017).

[61] J. Li, R. Fan, H. Wang, B. Ye, B. Zeng, H. Zhai, X. Peng, and J. Du, Measuring Out-of-Time-Order Correlators on a Nuclear Magnetic Resonance Quantum Simulator, Phys. Rev. X **7**, 031011 (2017).

[62] Z. Weinstein, S. P. Kelly, J. Marino, and E. Altman, Scrambling Transition in a Radiative Random Unitary Circuit, arXiv:2210.14242.

[63] X. Hu, T. Luo, and D. Zhang, Quantum algorithm for evaluating operator size with Bell measurements, Phys. Rev. A **107**, 022407 (2023).

[64] S. Pappalardi and J. Kurchan, Low temperature quantum bounds on simple models, SciPost Phys. **13**, 006 (2022).

[65] I. García-Mata, M. Saraceno, R. A. Jalabert, A. J. Roncaglia, and D. A. Wisniacki, Chaos Signatures in the Short and Long Time Behavior of the Out-of-Time Ordered Correlator, Phys. Rev. Lett. **121**, 210601 (2018).

[66] J. Wang, G. Benenti, G. Casati, and W. G. Wang, Quantum chaos and the correspondence principle, Phys. Rev. E **103**, L030201 (2021).

[67] R. A. Kidd, A. Safavi-Naini, and J. F. Corney, Saddle-point scrambling without thermalization, Phys. Rev. A **103**, 033304 (2021).

[68] V. Balachandran, G. Benenti, G. Casati, and D. Poletti, From the eigenstate thermalization hypothesis to algebraic relaxation of OTOCs in systems with conserved quantities, Phys. Rev. B **104**, 104306 (2021).

[69] J. Harris, B. Yan, and N. A. Sinitsyn, Benchmarking Information Scrambling, Phys. Rev. Lett. **129**, 050602 (2022).

[70] J. Braumüller *et al.*, Probing quantum information propagation with out-of-time-ordered correlators, Nat. Phys. **18**, 172 (2022).

[71] Y. L. Zhang, Y. Huang, and X. Chen, Information scrambling in chaotic systems with dissipation, Phys. Rev. B **99**, 014303 (2019).

[72] B. Yan and N. A. Sinitsyn, Recovery of Damaged Information and the Out-of-Time-Ordered Correlators, Phys. Rev. Lett. **125**, 040605 (2020).

[73] A. A. Patel, D. Chowdhury, S. Sachdev, and B. Swingle, Quantum Butterfly Effect in Weakly Interacting Diffusive Metals, Phys. Rev. X **7**, 031047 (2017).

[74] W. Zhao and R. Wang, Scaling laws of out-of-time-order correlators in a non-Hermitian kicked rotor model, Front. Phys. **11**, 1130225 (2023).

[75] B. Georgeot and D. L. Shepelyansky, Exponential Gain in Quantum Computing of Quantum Chaos and Localization, Phys. Rev. Lett. **86**, 2890 (2001).

[76] J. Gong and P. Brumer, Coherent Control of Quantum Chaotic Diffusion, Phys. Rev. Lett. **86**, 1741 (2001).

[77] A. Rajak, I. Dana, and E. G. Dalla Torre, Characterizations of prethermal states in periodically driven many-body systems with unbounded chaotic diffusion, Phys. Rev. B **100**, 100302(R) (2019).

[78] A. Kundu, A. Rajak, and T. Nag, Dynamics of fluctuation correlation in a periodically driven classical system, Phys. Rev. B **104**, 075161 (2021).

[79] L. Tamang, T. Nag, and T. Biswas, Floquet engineering of low-energy dispersions and dynamical localization in a periodically kicked three-band system, Phys. Rev. B **104**, 174308 (2021).

[80] T. Nag, S. Roy, A. Dutta, and D. Sen, Dynamical localization in a chain of hard core bosons under periodic driving, Phys. Rev. B **89**, 165425 (2014).

[81] K. Hashimoto, K. Murata, and R. Yoshii, Out-of-time-order correlators in quantum mechanics, J. High Energy Phys. 10 (2017) 138.

[82] S. Zamani, R. Jafari, and A. Langari, Out-of-time-order correlations and floquet dynamical quantum phase transition, Phys. Rev. B **105**, 094304 (2022).

[83] M. Gärttner, P. Hauke, and A. M. Rey, Relating Out-of-Time-Order Correlations to Entanglement via Multiple-Quantum Coherences, Phys. Rev. Lett. **120**, 040402 (2018).

[84] R. J. Lewis-Swan, A. Safavi-Naini, A. M. Kaufman, and A. M. Rey, Dynamics of Quantum Information, Nat. Rev. Phys. **1**, 627 (2019).

[85] W. L. Zhao, Quantization of out-of-time-ordered correlators in non-Hermitian chaotic systems, Phys. Rev. Res. **4**, 023004 (2022).

[86] L. Zhai and S. Yin, Out-of-time-ordered correlator in non-Hermitian quantum systems, Phys. Rev. B **102**, 054303 (2020).

[87] K. X. Wei, C. Ramanathan, and P. Cappellaro, Exploring Localization in Nuclear Spin Chains, Phys. Rev. Lett. **120**, 070501 (2018).

[88] X. Nie, Z. Zhang, X. Zhao, T. Xin, D. Lu, and J. Li, Detecting scrambling via statistical correlations between randomized measurements on an NMR quantum simulator, arXiv:1903.12237.

[89] K. A. Landsman, C. Figgatt, T. Schuster, N. M. Linke, B. Yoshida, N. Y. Yao, and C. Monroe, Verified quantum information scrambling, Nature (London) **567**, 61 (2019).

[90] S. K. Zhao, Z. Y. Ge, Z. Xiang, G. M. Xue, and S. P. Zhao, Probing Operator Spreading via Floquet Engineering in a Superconducting Circuit, Phys. Rev. Lett. **129**, 160602 (2022).

[91] G. Casati, B. V. Chirikov, F. M. Izrailev, and J. Ford, *Stochastic Behavior in Classical and Quantum Hamiltonian Systems*, edited by G. Casati and J. Ford, Lecture Notes in Physics Vol. 93 (Springer, Berlin, 1979).

[92] T. Mano and T. Ohtsuki, Machine learning the dynamics of quantum kicked rotor, Ann. Phys. (NY) **435**, 168500 (2021).

[93] See the Appendix for the details of LSTM method.

[94] X. Chen, T. Zhou, D. A. Huse, and E. Fradkin, Out-of-time-order correlations in many-body localized and thermal phases, Ann. Phys. (Leipzig) **529**, 1600332.

[95] B. Dóra and R. Moessner, Out-of-Time-Ordered Density Correlators in Luttinger Liquids, Phys. Rev. Lett. **119**, 026802 (2017).

[96] Y. Alavirad and A. Lavasani, Scrambling in the Dicke model, Phys. Rev. A **99**, 043602 (2019).

[97] B. Swingle, G. Bentsen, M. Schleier-Smith, and P. Hayden, Measuring the scrambling of quantum information, Phys. Rev. A **94**, 040302(R) (2016).

[98] G. Zhu, M. Hafezi, and T. Grover, Measurement of many-body chaos using a quantum clock, Phys. Rev. A **94**, 062329 (2016).

[99] M. Heyl, F. Pollmann, and B. Dóra, Detecting Equilibrium and Dynamical Quantum Phase Transitions in Ising Chains via Out-of-Time-Ordered Correlators, Phys. Rev. Lett. **121**, 016801 (2018).

[100] L. D'Alessio and M. Rigol, Long-time Behavior of Isolated Periodically Driven Interacting Lattice Systems, Phys. Rev. X **4**, 041048 (2014).

[101] W. L. Zhao, Y. Hu, Z. Li, and Q. Wang, Super-exponential growth of Out-of-time-ordered correlators, Phys. Rev. B **103**, 184311 (2021).

[102] R. Hamazaki, K. Fujimoto, and M. Ueda, Operator Noncommutativity and Irreversibility in Quantum Chaos, arXiv:1807.02360.

[103] F. M. Izrailev, Simple modelds of quantum chaos: spectrum and eigenfunctions, Phys. Rep. **196**, 299 (1990) and references therein.

[104] K. Q. Huang, J. Z. Wang, W. L. Zhao, and J. Liu, Chaotic dynamics of a non-Hermitian kicked particle, J. Phys.: Condens. Matter **33**, 055402 (2021).

[105] W. L. Zhao, P. K. Gong, J. Z. Wang, and Q. Wang, Chaotic dynamics of complex trajectory and its quantum signature, Chin. Phys. B **29**, 120302 (2020).

[106] S. Moudgalya, T. Devakul, C. W. von Keyserlingk, and S. L. Sondhi, Operator spreading in quantum maps, Phys. Rev. B **99**, 094312 (2019).

[107] T. Zhou, S. Xu, X. Chen, A. Guo, and B. Swingle, Operator Lévy Flight: Light Cones in Chaotic Long-Range Interacting Systems, Phys. Rev. Lett. **124**, 180601 (2020).

[108] K. X. Wei, P. Peng, O. Shtanko, I. Marvian, S. Lloyd, C. Ramanathan, and P. Cappellaro, Emergent Prethermalization Signatures in Out-of-Time Ordered Correlations, Phys. Rev. Lett. **123**, 090605 (2019).

[109] T. Boness, K. Kudo, and T. S. Monteiro, Doubly excited ferromagnetic spin-chain as a pair of coupled kicked rotors, Phys. Rev. E **81**, 046201 (2010).